

Copper Nanoparticles Coating on FTO with Improved Adhesion using Direct and Pulse Electrodeposition Techniques from a Simple Copper Sulphate Solution

(Salutan Nanozarah Kuprum pada FTO dengan Lekatan yang Diperbaiki menggunakan Teknik Elektrodeposisi Terus dan Nadi daripada Larutan Kuprum Sulfat Ringkas)

NUR AZLINA ADRIS¹, LORNA JEFFERY MINGGU^{1,*}, KHUZAIMAH ARIFIN^{1,2}, ROZAN MOHAMAD YUNUS¹,
MOHAMAD AZUWA MOHAMED^{1,3}, MASLIANA MUSLIMIN⁴ & MOHAMMAD B. KASSIM^{1,3}

¹*Fuel Cell Institute, Universiti Kebangsaan Malaysia, 43600 UKM Bangi, Selangor, Malaysia*

²*Research Center for Advanced Materials, National Research and Innovation Agency (BRIN), Building 224, KST BJ Habibie, South Tangerang 15314, Banten, Indonesia*

³*Department of Chemical Sciences, Faculty of Science and Technology, Universiti Kebangsaan Malaysia, 43600 UKM Bangi, Selangor, Malaysia*

⁴*Hydrogen Technology Unit, Materials Technology Group, Industrial Technology Division, Malaysian Nuclear Agency, 43000 Kajang, Selangor, Malaysia*

Received: 10 April 2023/Accepted: 14 July 2023

ABSTRACT

Copper (Cu) metal nanoparticles were deposited onto FTO glass using the electrodeposition method. The precursor used was $\text{CuSO}_4 \cdot 5\text{H}_2\text{O}$ with Na_2SO_4 as the inorganic additive. The formation of Cu was characterized using field emission scanning electron microscopy (FESEM), energy-dispersive X-ray spectroscopy (EDX), and X-ray diffraction (XRD). This study investigated the impacts of the electrodeposition method (direct electrodeposition vs. pulse electrodeposition), voltages (-0.4 V and -0.8 V), electrodeposition time (60s to 900s) and pulse cycles (50 cycles to 300 cycles), and FTO etching (fixed to 20s etching) towards the morphology and adhesion of Cu deposited. The grain size and thickness of Cu deposited vary with deposition time and pulse cycles. The voltage of -0.4 V successfully deposits shiny, metallic brown Cu onto FTO glass. Meanwhile, the voltage of -0.8 V gives powdery brown Cu on the surface. In addition, compared to direct electrodeposition (DD), pulse electrodeposition (PD) provides a more compact and homogeneous coverage of Cu onto FTO glass. The tape-test results also indicate that FTO etching by electrolysis reduction can improve the adhesion strength between deposited thin Cu film and the FTO glass. This work demonstrates a facile electrodeposition technique with substrate etching as an effective deposition of Cu metal with the potential for application in a wide range of fields.

Keywords: Adhesion; copper; electrodeposition; inorganic additive; FTO glass

ABSTRAK

Nanozarah logam kuprum (Cu) diendapkan di atas kaca FTO menggunakan kaedah pengendapan elektrokimia. Prekursor yang digunakan ialah $\text{CuSO}_4 \cdot 5\text{H}_2\text{O}$ dan Na_2SO_4 sebagai bahan tambah tidak organik. Pembentukan Cu dicirikan menggunakan mikroskop elektron pengimbasan pelepasan medan (FESEM), spektroskopi sinar-X penyebaran tenaga (EDX) dan pembelauan sinar-X (XRD). Penyelidikan ini mengkaji kesan kaedah elektroendapan (elektroendapan langsung lawan elektroendapan denyutan), voltan (-0.4 V dan -0.8 V), masa elektroendapan (60s dan 900s) dan kitaran denyutan (50 hingga 300 kitaran) dan punaran FTO (ditetapkan selama 20s) terhadap morfologi dan lekatan Cu yang diendapkan. Saiz butiran dan ketebalan Cu yang diendapkan berbeza mengikut masa endapan dan kitaran denyutan. Voltan -0.4 V berjaya mengendapkan Cu coklat metalik berkilat pada kaca FTO. Sementara itu, voltan -0.8 V memberikan Cu coklat serbuk pada permukaan. Di samping itu, berbanding dengan elektroendapan langsung (DD), Elektroendapan denyutan (PD) memberikan liputan Cu yang lebih padat dan homogen di atas kaca FTO. Keputusan ujian pita juga menunjukkan bahawa FTO yang dipunarkan melalui penurunan elektrolisis boleh meningkatkan kekuatan lekatan antara filem Cu nipis terendap dan kaca FTO. Kajian ini menunjukkan teknik elektroendapan yang mudah dengan punaran substrat bagi endapan logam Cu yang berkesan dengan potensi untuk digunakan dalam pelbagai bidang.

Kata kunci: Bahan tambah tidak organik; elektroendapan; kaca FTO; kuprum; lekatan

INTRODUCTION

Electrodeposition is a well-established technology for *in situ* deposition of various metallic materials on a substrate with a facile and low-cost approach. It is accomplished by passing an electric current through a conductive material immersed in a solution containing a salt of the metal to be deposited. It is a versatile and cost-effective technology for fabricating a wide variety of two- and three-dimensional materials, including coatings and thin film (Nasirpouri et al. 2020). Electrodeposition involves the reduction or deposition of electroactive on the cathode surface (Tarditi, Bosko & Cornaglia 2017). It has been widely used in the fabrication of thin films with various morphology, such as nanowires (Schiavi et al. 2019), nanorods (Kim et al. 2020; Rasouli, Rouhollahi & Ghahramanifard 2019), and nanoparticles (Braesch et al. 2020; Chen et al. 2019; Jothi, Jaganathan & Nageswaran 2020; Pan et al. 2020).

Copper (Cu) electrodeposition has been used to fabricate thin films ranging in thickness from micrometres to nanometres for various purposes. It is widely used to manufacture electrical and electronic device components such as semiconductor chip interconnectors (Calcutt 2001). Apart from electrical uses, Cu metal is also utilized in construction, interior design, and other areas of architecture (Schnebele et al. 2019). Cu-based nanostructures have garnered significant interest in recent years as a potential catalyst and electrocatalyst for both oxygen evolution reaction (OER) and hydrogen evolution reaction (HER) (Danilovic et al. 2012; Kannimuthu et al. 2021; Rajput, Kundu & Chakraborty 2021). Additionally, Cu has been used as an interconnected metallic core beneath a metal oxide to boost the conductivity of the metal oxides (Maduraiveeran, Sasidharan & Jin 2019; Rajput, Kundu & Chakraborty 2021; Veerakumar et al. 2020).

Besides, Cu can also be deposited on a substrate as starting material for the fabrication of copper hydroxide nanowires (Borkar et al. 2018; Luo et al. 2016; Toupin et al. 2017). Besides industrial applications, Cu has been demonstrated to be a promising photocatalyst, advantageous for solar cell, capacitor and photoelectrochemistry applications. Others have studied the mechanism of Cu ion reduction on several substrates, including ITO and FTO glass, silicon, graphene, platinum, and glassy carbon electrode (Aravinda, Mayanna & Muralidharan 2000; Jaikumar et al. 2015; Khaniche, Zouaoui & Zegadi 2020; Rana, Rahman & Alam 2014). However, few studies have been conducted on Cu electrodeposition on fluorine

tin oxide (FTO) glass. FTO glass is notable for its low-cost, high electronic conductivity, electrochemical stability, thermal stability, and optical transparency, thus commonly being utilized as an attractive substrate for photoelectrochemical water splitting (PEC), dye-sensitized solar cells (DSSCs) and other electrocatalytic systems (Tang, Chakthranont & Jaramillo 2017; Wang et al. 2020).

In addition, industrial methods for Cu deposition frequently include toxic additive chemicals such as malachite green (Han, Zhang & Leach 2014), ethylene diamine (Gu et al. 2012), sulfuric acid (Haba, Ikeda & Uosaki 2019; Tao et al. 2021) as the accelerators, suppressants, inhibitors, or levellers. As an alternative, sodium sulfate (Na_2SO_4) has been used as an additive, mainly due to its non-toxic, non-hazardous, and chemically very stable. The Na_2SO_4 additive help to increase the conductance of the bath solution by increasing the ionic strength of the solution for electrodeposition of copper (Khaniche, Zouaoui & Zegadi 2020; Tran et al. 2020) and other materials (Shivakumara et al. 2007; Xu et al. 2021). As a result of employing these additives, the grain size and grain boundaries of the copper deposits are decreased while the morphology of the deposits' surfaces is enhanced (Gu et al. 2012; Sekar 2017). Without additives during electroplating, copper will be plated more heavily on the corner, causing pinching (Adolf 2008). Therefore, additives play an essential role in copper electrodeposition.

FTO (Fluorine-doped Tin Oxide) glass is a transparent conductive glass with unique features and widely used in semiconductor research. The fundamental rationale for choosing FTO glass is that it is highly conductive and translucent. As a result, it is perfect for use as a substrate material in a wide range of semiconductor applications, including solar cells, thin-film transistors, and other electronic devices (Alfadhli et al. 2023; Chang et al. 2021; Li et al. 2019; Oo et al. 2012). FTO glass is also highly stable and resistant to high temperatures, making it excellent for fabricating these semiconductor devices (Chaitra et al. 2021; Zhao et al. 2019). Furthermore, FTO glass is generally inexpensive and straightforward, making it an appealing choice for researchers and manufacturers.

However, FTO etching may result in a better film deposition, as it modifies the surface of the substrate and allows high adhesion of metallic coatings to the substrate (Bae et al. 2015). Etching serves the purpose of removing the oxide layer on the surface of the substrate and raising the surface roughness level, both of which

contribute to an increase in the adherence of the deposit to the substrate (Kotok et al. 2017). There are many ways of substrate etching, such as chemical etching (Keshtmand et al. 2021; Zhang et al. 2019), electrochemical etching (Bae et al. 2015; Kotok et al. 2017; Toupin et al. 2017), and laser etching (Huang et al. 2021; Ren et al. 2021). The chemical etching process involves more complicated techniques, even though it is one of the cost-effective procedures. This is because of the chemical inertness features of the chemicals involved (Lee et al. 2014). Thus, the electrochemical method, which involves a simple process, is more favorable.

Here we report a facile electrodeposition method for Cu using sodium sulfate as an additive. Besides, this study also investigates the effect of direct voltage electrodeposition (DD) and pulsed voltage electrodeposition (PD) for metallic Cu onto FTO glass. The influence of FTO glass etching is also included to study the adhesion strength between deposited Cu metal and the FTO glass. Well-deposited Cu thin film is significant as Cu underlayers can help reduce contact resistance and improve electrical conductivity between the semiconductor layer and the substrate.

MATERIALS AND METHODS

MATERIALS

All chemicals were of analytical grades and used without further purification. Copper sulfate pentahydrate ($\text{CuSO}_4 \cdot 5\text{H}_2\text{O}$) and acetone were purchased from R&M Chemicals. Sodium sulfate (Na_2SO_4) and sulfuric acid (H_2SO_4) were purchased from Sigma-Aldrich. Ethanol was purchased from QReC. All solutions were prepared with deionized water. The fluorine-doped tin oxide (FTO) glass with a thickness of 2.2 mm and resistance of 7 Ohm (Solaronix, Switzerland) was used as the conductive substrate, cut using a glass cutter (Zhuhai Kaivo Optoelectronic Technology) into $2.5 \times 1.0 \text{ cm}^2$ size each. A platinum mesh was used as the counter electrode, and Ag/AgCl saturated in 3 M KCl was used as the reference electrode. Copper tape and Teflon tape were used for electrodeposition purposes. Electrodeposition was performed using Ametek Versastat 4 instrument.

Cu ELECTRODEPOSITION

The thin Cu films were electrochemically deposited onto FTO glass from a sulfate solution containing 0.01 M $\text{CuSO}_4 \cdot 5\text{H}_2\text{O}$ and 0.2 M Na_2SO_4 in deionized water. Before electrodeposition, FTO glass was cleaned with

acetone, ethanol, and deionized water for 5 minutes ultrasonically in each solvent. Then, Cu tape was attached to the top edge conductive surface of the cleaned FTO glass for better conductivity, which was then covered with Teflon tape to expose approximately $1.0 \times 1.0 \text{ cm}^2$ of the substrate.

Initially, cyclic voltammetry (CV) was performed to determine the electrodeposition voltage of Cu on the FTO glass. The CV was conducted in the prepared electrolyte solution in a voltage window of -1.0 to +1.0 V with respect to the saturated Ag/AgCl reference electrode. Next, thin Cu films were deposited on FTO by using either DD or PD at room temperature and specific electrodeposition time with a three-electrode configuration system, where blank FTO glass serves as the working electrode, platinum mesh as the counter electrode, and Ag/AgCl saturated in 3 M KCl as the reference electrode. The solution was stirred continuously with a magnetic stir at 150 rpm. The sample was then rinsed thoroughly with deionized water and dried at room temperature.

The applied voltage is switched on and off repeatedly for the sample prepared by PD, in contrast to the one prepared by DD, where a constant voltage is applied. After electrodeposition, the electrode was rinsed with deionized water and dried in the air. The applied voltage (-0.4 & -0.8 V), electrodeposition time (50 & 600 s) and electrodeposition cycles (50 & 200 cycles) were varied, respectively, to investigate these effects towards Cu growth on FTO. The direct electrodeposition and pulse electrodeposition samples were labelled as DD-time or PD-cycle. In contrast, for etched FTO, the samples were labelled as DD-time-E or PD-cycle-E.

FTO SUBSTRATE ETCHING

To study Cu adhesion on the substrate, etching of the FTO substrate was conducted with a solution of 0.01 M Na_2SO_4 and 0.1 M H_2SO_4 in deionized water under a cathodic current of -25 mA/cm^2 for 20 s, as reported from previous work (Toupin et al. 2017). Then, Cu was electrodeposited on the etched FTO using the abovementioned method.

CHARACTERIZATION

The surface morphology and cross-sections of the FTO/Cu samples were examined using a field emission scanning electron microscope (FESEM) (Zeiss AM10) which is equipped with energy dispersive X-ray spectroscopy (EDX) to analyse surface elemental

composition. The chemical composition and crystalline structure of the samples were analysed using an X-ray diffractometer (Model PANalytical XPert Pro MPD, Cu $K\alpha$ irradiation, $\lambda = 1.5405 \text{ \AA}$). The electrical conductivity test was performed using Jandel Multi Height Four Point Probe attached with the RM 3 Test Unit. The adhesion of electrodeposited Cu on FTO glass was tested using the tape-test method specified in ASTM D3359-02 (Kim et al. 2020).

RESULTS AND DISCUSSION

ELECTRODEPOSITION VOLTAGE DETERMINATION

The electrochemical studies of copper sulfate in different applied voltages have been conducted using the cyclic voltammetry technique. In the present study, preliminary potentiodynamic experiments were performed using cyclic voltammetry to examine the electrochemical reduction voltage of Cu ions. The cyclic voltammogram (CV) in Figure 1 shows a symmetric reduction and oxidation peaks which indicates Cu deposition, and Cu stripping, respectively. A similar shape of CV was reported earlier by Mentar (2011) using $\text{CuSO}_4 \cdot 5\text{H}_2\text{O}$ as the electrolyte. The CV was acquired by sweeping towards negative voltages and then reversing with a slow voltage scan rate of 5 mV/s. Under the influence of applied voltage, the Cu^{2+} ions are reduced at the cathode for the formation of copper film on the FTO, whereas water will be oxidized at the anode to form oxygen gas and H^+ ions (Dubale et al. 2015).

As shown in Figure 1, there was no current produced initially, until potential of 0.02 V and 0.06 V were reached for blank and etched FTO, respectively. The cathodic current starts to increase and forms peak at -0.24 V for blank FTO and 0.35 V for etched FTO on the forward scan, which can be associated with Cu deposition on FTO due to the reduction of Cu^{2+} to Cu. The reverse scan reconfirms the deposition reaction. The cathodic current then started to decrease and turns into anodic current. A crossover was observed between the cathodic and anodic current where the nuclei was formed on the electrode due to the difference in deposition and dissolution potentials (Grujicic & Pesic 2002; Smith, Campbell & Walsh 1995). This is because, when metallic ions are deposited onto a substrate with different material, the mismatch in crystallographic parameters between the ions and the substrate introduces strain and energetically unfavourable interactions at the interface. This strain and mismatch can impede the nucleation and growth of the deposited metal ions on the substrate surface. As a result, a higher potential is required to overcome these energy barriers and initiate the deposition process (Grujicic & Pesic 2002). The anodic peak is then observed in the voltage range of 0.28 V (blank FTO) and 0.48 V (etched FTO), which can be associated with Cu stripping due to the oxidation of Cu to Cu^{2+} (Böhme et al. 2019). Thus, the voltage of -0.4 V was selected for Cu metal electrodeposition on FTO glass. Another voltage of -0.8 V was also tested as a comparison for Cu metal electrodeposition at more cathodic voltage

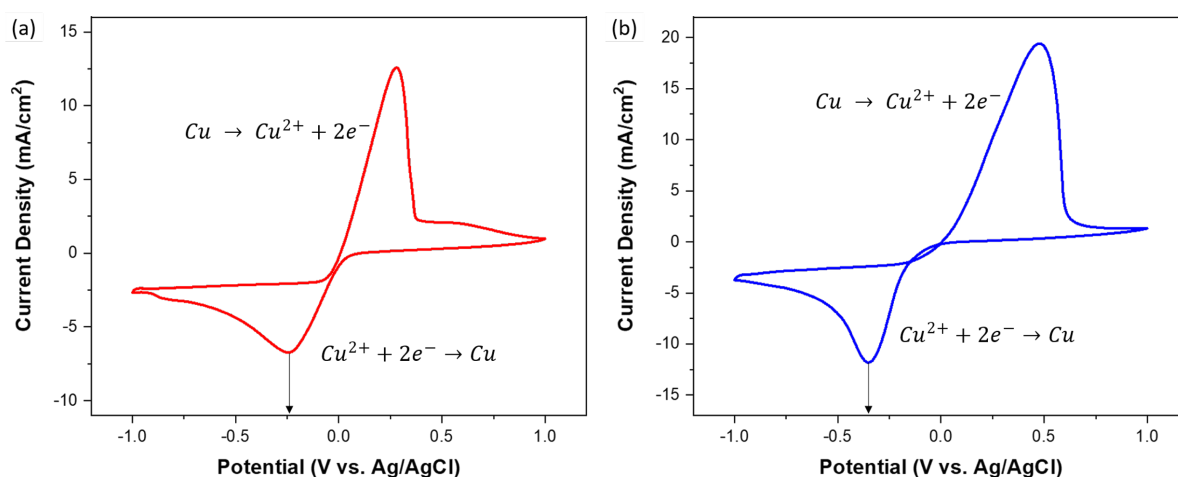


FIGURE 1. Cyclic voltammogram of (a) blank FTO and (b) etched FTO in 0.01 M $\text{CuSO}_4 \cdot 5\text{H}_2\text{O}$ and 0.2 M Na_2SO_4 precursor solution at a voltage scan rate of 5 mV/s

(He et al. 2018). Hence, the electrodeposition was performed by applying the selected voltages for different deposition times and cycles to study the effect of those parameters towards the growth of Cu on the FTO glass.

THE IMPACT OF VARIOUS ELECTRODEPOSITION PARAMETER ON Cu DEPOSITION ON FTO

The experimental setup for DD is the same as that used for PD, as shown in Figure 2(a). The FESEM surface and cross-section morphology images of the Cu samples deposited on unetched FTO obtained by DD and PD with varying electrodeposition time and voltage are

shown in Figures 3 and 4, respectively. The Cu thin film was deposited with pulse electrodeposition (PD) mode with pulse waveform for electrodeposition at duty cycle 67% where the T_{on} and T_{off} are 2 and 1 second, respectively (Vuong et al. 2020). The PD enables the incorporation of higher concentrations of nanoparticles as well as producing a wider range of deposit compositions and properties (Odetola et al. 2016). The visually observed thin metallic brown film grown on the FTO glass, as shown in Figure 2(b), indicates the characteristic of the presence of Cu, as reported by other works (Kaewvilai et al. 2017; Mathur 2013). However, the visual image of FTO/Cu is found to vary depending on the parameters tested.

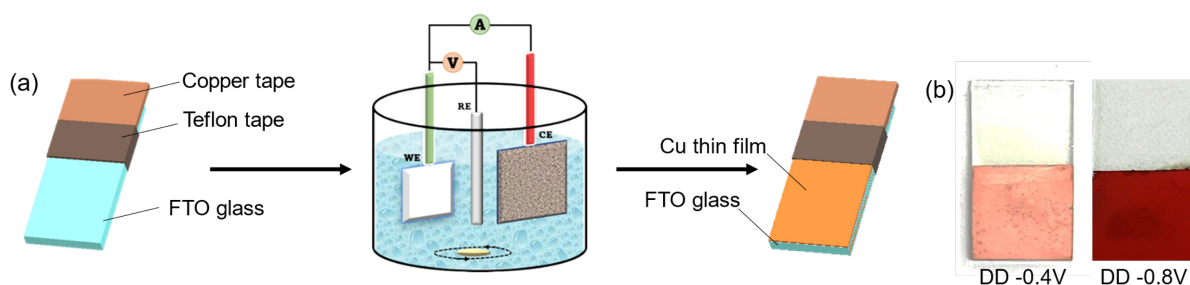


FIGURE 2. (a) FTO/Cu electrodeposition setup, and (b) the photograph image of Cu deposited via direct voltage electrodeposition (DD) at the voltage of -0.4 V (metallic brown) and -0.8 V (dark brown). (*Cu deposited via pulsed voltage electrodeposition (PD) also have similar color shades as DD)

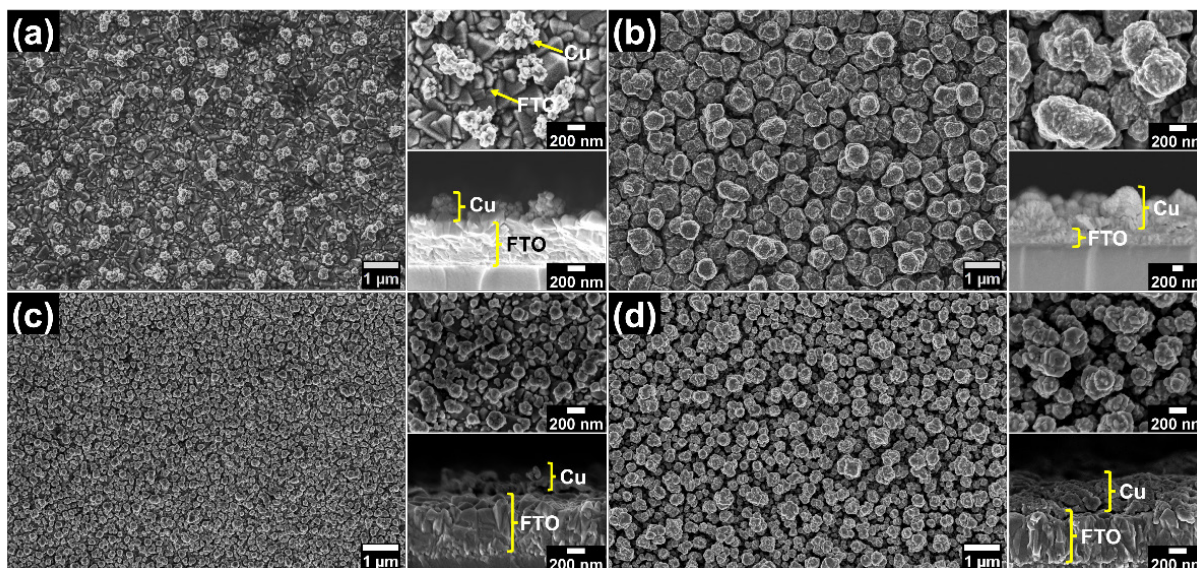


FIGURE 3. FESEM images of FTO/Cu thin film prepared by direct electrodeposition at -0.4 V for (a) DD-60s, (b) DD-600s, and at -0.8 V for (c) DD-60s, and (d) DD-600s viewed at low to high (10k & 50k) magnification with its crosssection morphology viewed at 50k magnification

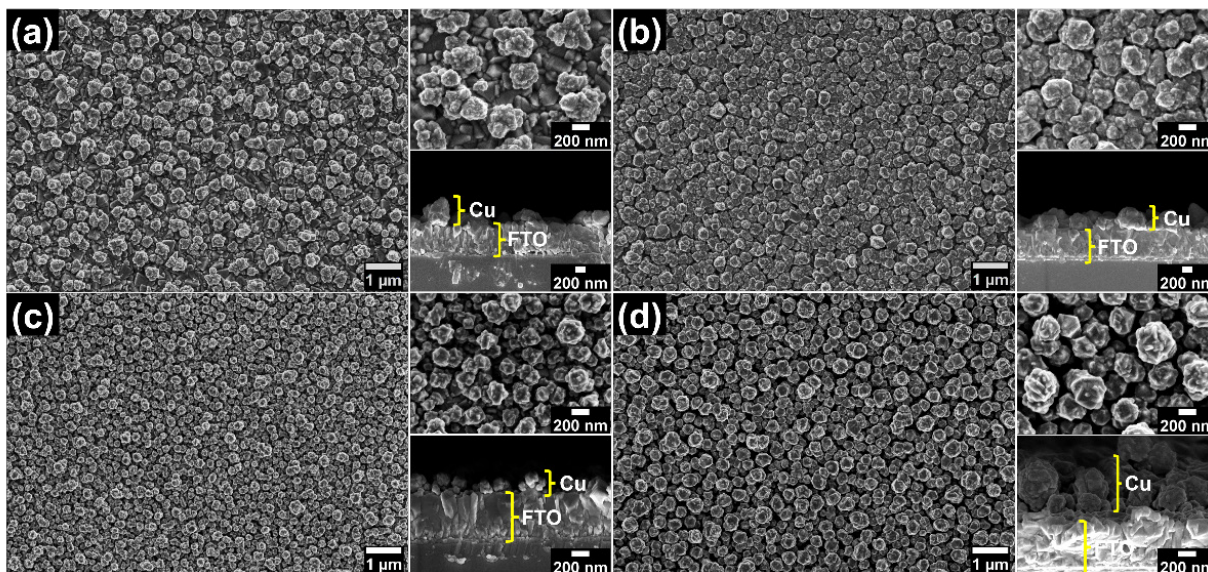


FIGURE 4. FESEM images of FTO/Cu thin film prepared by pulse electrodeposition at -0.4 V for (a) PD-50cyc, (b) PD-200cyc, and at -0.8 V for (c) PD-50cyc, and (d) PD-200cyc viewed at low to high (10k & 50k) magnification with its crosssection morphology viewed at 50k magnification

A metallic brown film of Cu was observed when electrodeposited at a less cathodic voltage of -0.4 V for FTO/Cu using direct deposition (DD-60s). Meanwhile, FESEM image in Figure 3(a) shows that traces of irregular Cu nanoparticles were about to grow on the FTO glass. The nanoparticles are like tiny irregular structures with an average particle size of 231 nm and layer thickness of 242 nm. Figure 3(b) shows that for FTO/Cu at longer deposition time (DD-600s), uniform coverage of nanoparticle structures was grown on the FTO glass. This shape is similar to other reported studies where Cu nano spherical structure was seen deposited onto FTO glass at slightly higher voltage and different supporting electrolytes (He et al. 2018; Khelladi et al. 2009; Mandke & Pathan 2012; Riveros et al. 2020). The nano spherical structure seems to grow bigger with an average particle size of 535 nm and layer thickness of 732 nm at a longer deposition time, as shown in Table 1 and Figure 3. This result is similar to other reported studies, where particle diameters increase with the electrodeposition time at a constant voltage or current density (Olson, Atanassov & Brevnov 2005; Yun et al. 2008).

Meanwhile, for FTO/Cu direct electrodeposition at the more cathodic voltage of -0.8 V, a powdery dark brown thin film was deposited onto FTO glass (Figure 1(b)). Previous work also reported similar dark brown

Cu film at high cathodic deposition (Norziehana et al. 2017; Sadana, Deshpande & Gedye 1982). For DD with lower duration (DD-60s) at -0.8 V, the Cu obtained is rather nano-spherical in shape with an average particle size of 196 nm and layer thickness of 101 nm (Figure 3(c)). The Cu particle deposited at -0.8 V is well covered compared to sparsely covered for DD at -0.4 V for the same 60 s. Higher deposition voltage increased the nucleation rate hence more sites for the particles to grow (Mladenović et al. 2022). Even though at -0.8 V, the Cu has well covered the FTO, but the particle size is smaller compared to Cu deposited at -0.4 V. As for the higher duration (DD-600s) at -0.8 V, the Cu particles have grown more prominent with an average particle size of 327 nm and layer thickness of 415 nm (Figure 3(d)). The particle size is also smaller at -0.8 V compared to -0.4 V for 600 s direct electrodeposition. While higher deposition voltage with sufficient induction time tends to produce dendritic-shaped Cu particles (He et al. 2018; Nikolić & Popov 2010), it seems that in this study, at -0.4 V (600 s) and -0.8 V (600 s), dendritic growth is not apparent. The dendritic structure is reported to be caused by mass-transport limited growth where Cu(II) is depleted near the electrode due to a high reduction rate causing preferential deposition along tip edges forming dendrites (Bakthavatsalam et al. 2016; Qiu et al. 2009).

TABLE 1. Properties of electrodeposited Cu onto FTO substrate with its various electrodeposition parameters

FTO/Cu	Deposition voltage (-0.4V)		FTO/Cu	Deposition voltage (-0.8V)	
	Particle size (nm)	Crystallite size (nm)		Particle size (nm)	Crystallite size (nm)
DD-60s	231	8	DD-60s	196	16
DD-600s	535	25	DD-600s	327	40
DD-600s-E	311	12	DD-600s-E	263	14
PD-50cyc	336	16	PD-50cyc	202	25
PD-200cyc	360	33	PD-200cyc	304	36
PD-200cyc-E	291	10	PD-200cyc-E	234	13

*Average particle size was determined from SEM while crystallite size determined using Debye-Scherrer equation from XRD data. Explanation on crystallite size is further discussed in the XRD section below (E - indicates etching of FTO was performed prior to Cu electrodeposition)

The effect of the PD method towards Cu growth is also being investigated in this study. Thin Cu film has been deposited with the same voltages used for DD but with different pulse cycles (50, 100, 150, 200 and 300 cycles with T_{on} and T_{off} of 2s and 1s for each cycle). Pulse voltage deposition is similar to pulsing reverse current deposition as the output reverses current (Pavlović et al. 2010). The PD of Cu at -0.4 V for 50 cycles (PD-50cyc) results in the formation of a thin metallic brown film deposited onto the FTO glass similar to DD at the same voltage, indicating the growth of Cu on the FTO. This is supported through FESEM images in Figure 4(a), where irregularly shaped Cu nanoparticles grew sparsely on the FTO glass with an average particle size of 336 nm and layer thickness of 267 nm. When deposited with higher cycles (PD-200cyc), the Cu formed bigger and coarser particles, as shown in Figure 4(b). The Cu nanoparticles produced an average particle size of 360 nm and layer thickness of 410 nm. The total on time for PD-200cyc is similar to DD-600s. It can be seen that PD-200cyc at -0.4 V (Figure 4(b)) produced more compact and finer particles than DD-600s (Figure 3(b)). PD has been reported to enable replenishment of Cu(II) from bulk electrolyte transported to the electrode during off time, which enhanced nucleation rate during on time, producing smaller particle size and more compact deposit (Das et al. 2022; Esmaili, Bahrololoom & Kavanagh 2011; Gyftou, Pavlatou & Spyrellis 2008; Wahyudi et al. 2019). It is also reported that in the pulse voltage deposition, there is a reverse

current during off-time, causing the dissolution of lower tip radii than larger ones resulting in blunted edges. Many nuclei also dissolved during the reverse current, which enables growth at lower sites resulting in a larger particle (Pavlović et al. 2010).

Meanwhile, for PD at the more cathodic voltage of -0.8 V, a powdery dark brown thin film was deposited onto FTO glass like DD at a similar voltage. Figure 4(c) shows that PD-50cyc at -0.8 V has a rather nano spherical-shaped Cu deposited on FTO glass with an average grain size of 202 nm and layer thickness of 206 nm. As for PD-200cyc, the Cu nanoparticle has grown more prominent, as shown in Figure 4(d), with an average particle size of 304 nm and layer thickness of 593 nm. The particle size and layer thickness of Cu nanoparticles deposited via PD increase with increasing deposition cycles (Figure 4), similar to the effect of deposition time on DD, where the grain size of Cu deposited at a longer time is more prominent than those deposited at a shorter time (Figure 3). Besides this, the dissolution due to the reverse current also affects the PD morphology, as mentioned above, for -0.4 V PD.

The XRD patterns of the FTO/Cu DD and PD shown in Figure 5(a) indicates that the nanoparticles grown on the FTO glass surface were Cu in the metallic phase (Cu₀). The diffraction peak of (111), (200), and (220) at 43.29°, 50.5° and 74.1° represents Cu (JCPD 04 836); meanwhile, other peaks represent the FTO glass (He et al. 2018; Li, Natsuki & Natsuki 2021; Toupin et al. 2017). Deposition at the longer time and higher cycles (600 s &

200 cycles) for both -0.4 and -0.8 V shows a small peak for Cu_2O . The PD-200cyc consists of a minute Cu_2O peak (0.6 % for -0.4 V and 0.3 % for -0.8 V), compared to the DD-600s, which consists of a higher amount of Cu_2O (2.5 % for -0.4 V and 3.4 % for -0.8 V) where the percentage was estimated based on XRD data using Rietveld method with HighScore software. The ratio of Cu (II)/Cu (0) for -0.8 V is 4:96 (DD) and 1:99 (PD) compared to 3:97 (DD) and 1:99 (PD) for -0.4 V. This peak is most likely not CuO as it is more related to the dominant peak of Cu_2O (Jeong et al. 2022). The XRD diffractogram of Cu

electrodeposition at 600 s and 200 cycles shows a higher intensity peak of Cu compared to 50 s and 50 cycles deposition, in this case, due to the much higher amount of Cu being electrodeposited onto FTO glass with higher time and cycles. The increased Cu coverage and thickness with deposition time and the cycle are also shown by FESEM images (Figures 3 & 4). Both DD and PD show (111) as the most dominant peak. This is consistent with other reports where the (111) is the preferred plane as it has the lowest surface energy (He et al. 2018; Pavlović et al. 2010; Zhao et al. 2017).

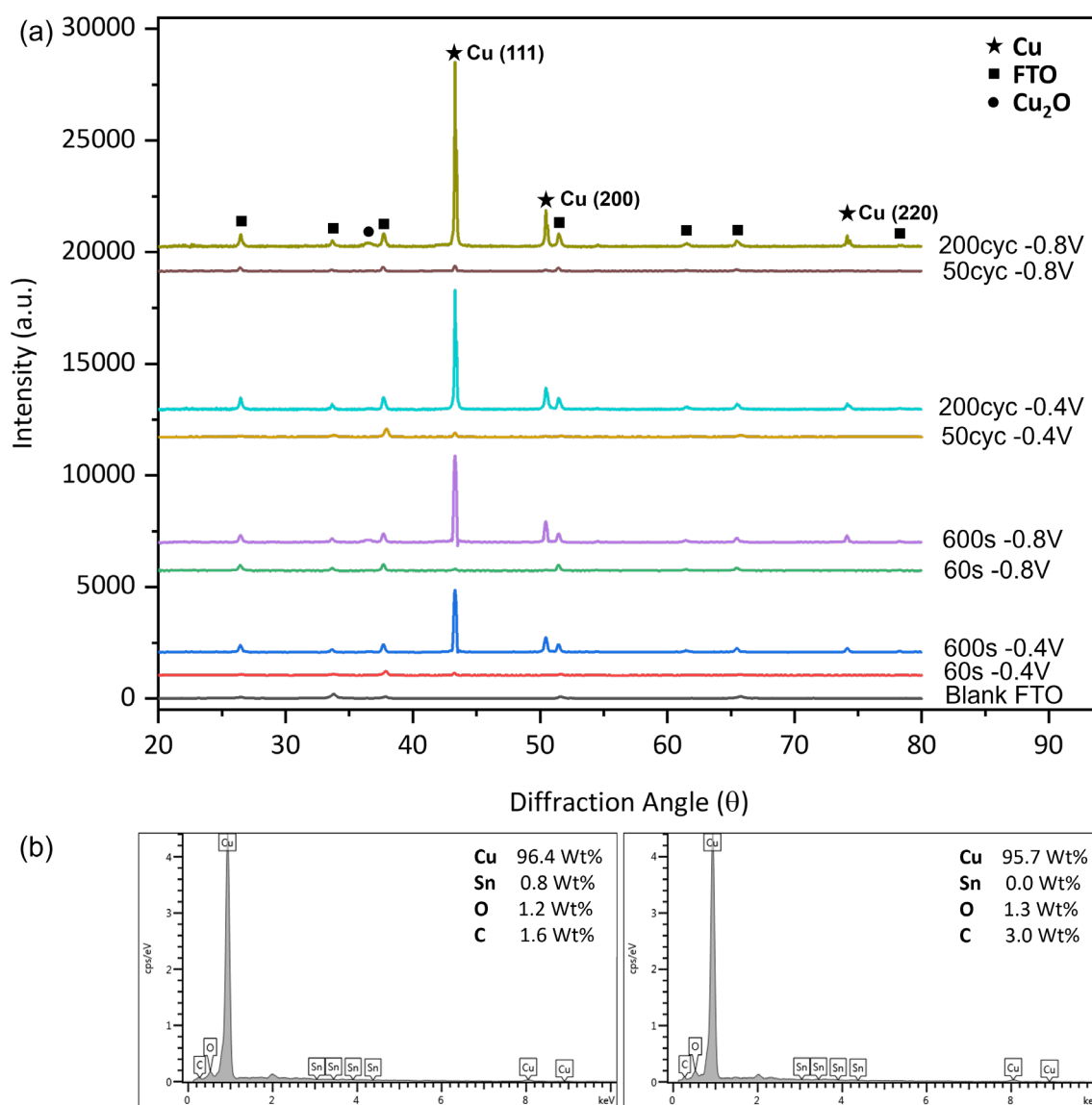


FIGURE 5. (a) XRD Spectra of the FTO/Cu prepared via DD and PD on blank FTO substrate, and EDX spectrum of (b) FTO/Cu DD at -0.4 V (left) and at -0.8 V (right) (*FTO/Cu PD has similar EDX pattern)

In general, the particle size determined by FESEM analysis is significantly larger than the crystallite size determined by XRD (Table 1). This is because the particle size observed in the FESEM images above pertains to a particle that may be composed of multiple crystallites or a single crystallite. In the meantime, crystallite size refers to the measurement of regions/domains of a material that diffract coherently. Utilising the Debye-Scherrer equation, the size of crystallites was determined. Similar to what has been reported for particle size, it has been observed that the size of crystallites increases with increasing electrodeposition time and pulse cycles. This may be the result of more time for nucleation and growth processes to occur, allowing the crystallite to develop continuously until its size increases (Zhang et al. 2015). Consequently, a longer deposition time and cycle can result in a larger crystallite size. Nevertheless, FESEM analysis shows that the particle size of Cu deposited at higher cathodic voltage is smaller, whereas XRD analysis shows that the crystallite size of Cu deposited at higher cathodic voltage is marginally larger. This may be a result of the higher formation voltage, which allowed the crystallites more time to develop, resulting in their enlargement. As a result of an increase in the deposition voltage, an increase in the size of crystallites has also been observed in previous studies (Li & Zhang 2020; Rashidi & Amadeh 2008).

EDX analysis was also used to analyse the elemental composition of the nanostructured Cu, as shown in Figure 5(b) for DD and PD, respectively. Cu is assigned to the peaks at 0.91, 8.03, and 8.89 keV, similar to those reported in other papers (Alshehri & Malik 2020; Babouri et al. 2019). Other peaks labelled as C may come from the carbon adhesive tape used during analysis (Taheraslani & Gardeniers 2019); meanwhile, peaks labelled as Sn and O come from the FTO glass. The elemental composition obtained from EDX analysis is consistent with the diffractogram obtained from XRD.

THE IMPACT OF FTO ETCHING ON Cu DEPOSITION, MORPHOLOGY, AND ADHESION PROPERTIES

FTO glass etching before electrodeposition was also conducted to determine the effect of the etching step towards morphology and substrate adhesion. FESEM images shown in Figure 6(a)6(b) represents the morphology of the FTO glass surface before and after etching. The blank FTO glass before the etching process has closely packed nanoparticles. While the FTO glass that has undergone etching has a porous surface, as shown in Figure 6(b) (inset). The conductivity of FTO

obtained from four-point probe system decreased slightly from 0.11 S/cm blank to 0.08 S/cm after etching. However, increased surface roughness of FTO substrate facilitates in enhanced electrodeposition process, improved adhesion between the deposited material and the substrate, and thus exhibit improved electrocatalytic activity compared to the smooth surfaces (Liu et al. 1994; Qing et al. 2017; Toupin et al. 2017).

The etched FTO glass was then used to electrodeposit Cu using the abovementioned method at -0.4 and -0.8 V for DD-600s and PD-200cyc, respectively. In terms of Cu morphology, the particle shape is similar for etched DD-600s-E at -0.4 V (Figure 6(c)) and unetched DD-600s (Figure 3(b)) which shows the nano spherical structure. The morphology for etched PD-200cyc-E at -0.4 V (Figure 6(d)) shows the aggregate of distinct particles with blunted edges, while unetched PD-200cyc has relatively spherical particles (Figure 4(b)). Meanwhile, for etched DD-600s-E at -0.8 V (Figure 6(e)), the morphology shows the aggregate of distinct particles but with sharp edges. Under PD at -0.8 V (PD-200cyc-E), the morphology is similar to DD at the same voltage, but the particles are less distinct with rounded edges (Figure 6(f)). The electrodeposited Cu particle structure is affected by the reaction mechanism at the electrode, such as charge transfer and mass transport rates (Pavlović et al. 2010). The particle size of Cu for direct and pulse deposition on etched FTO at -0.4 V (311 nm DD, 291 nm PD) is more prominent than at -0.8 V (263 nm DD, 234 nm PD). This is due to a higher voltage which induced a higher nucleation rate producing smaller particle size, as mentioned in the discussion for Cu deposition on unetched FTO. The film thickness of Cu on etched FTO at -0.4 V is 457 and 568 nm, while at -0.8 V is 674 and 695 nm for DD and PD, respectively. However, etched FTO/Cu at -0.8 V shows thicker films due to the cluster growth of Cu (Figure 6(e) & 6(f)). The etching of FTO affects the morphology, especially for DD and PD at -0.8 V (Figure 6(e) & 6(f)). As shown in Figure 6(b), the FTO surface is relatively porous after etching, which increases the surface area and provides more nucleation sites. The Cu grown on etched FTO has smaller particle and crystallite size than unetched FTO (Table 1).

The XRD of the etched blank FTO and Cu electrodeposited on etched FTO are shown in Figure 7(a). The XRD of blank FTO shows peaks of SnO₂. After etching, the XRD shows additional Sn peak at 30°, along with other SnO₂ peaks (similar as blank FTO). The XRD peak of etched FTO is similar to that reported by More

and Bhargava (2017). However, after Cu deposition, the Sn peak is undetected and only shows peaks for FTO (SnO_2) and metallic Cu with (111) as the most dominant peak. Etching also exposed the SnO_2 peak at 78° compared to unetched FTO. The peak for Cu_2O is not detected for deposition on etched FTO glass even at the longer time and higher cycle (600 s & 200 cycles) for both DD and PD (-0.4 & -0.8 V). This contrasts unetched FTO, where a small Cu_2O peak was detected when deposited at a longer time and higher cycles. The elemental composition obtained from EDX analysis (Figure 7(b)) is consistent with the diffractogram obtained from XRD analysis. The XRD peaks intensity of electrodeposited Cu on etched FTO (600 s & 200 cycles) for both deposition voltages are similar to peaks intensity on unetched FTO for low time & cycles (60 s & 50 cycles), where the FTO peaks are more dominant than the Cu peaks. This contrasts with the unetched FTO/Cu peak (600 s & 200 cycles), where the Cu peak intensity is much higher than the FTO peaks for both deposition voltages of -0.4 and -0.8 V (Figure 5(a)).

Mainly, the XRD of the Cu deposited on etched FTO shows lower peak intensity compared to Cu on unetched FTO. Although the etched FTO/Cu has a higher total charge for electrodeposition (-0.4 V ~703 mC; -0.8 V ~611 mC) than unetched FTO/Cu (-0.4 V ~395 mC; -0.8 V ~302 mC) for DD. The reduced intensity of XRD peaks could indicate reduced crystallinity of the Cu deposited on etched FTO compared to the unetched FTO at similar deposition voltage and time. It could also be due to the porous FTO where Cu is deposited inside the FTO structure apart from on the surface (Khan et al. 2020). The crystallite size calculated from the Debye-Scherrer equation shows that Cu deposited on etched FTO has the smallest size (Table 1). The adherence of a thin Cu film on FTO glass was also investigated using the tape-test methodology following ASTM D3359-02. The thin Cu films were deposited on both unetched and etched FTO to study the effect of electrolysis reduction of FTO glass before electrodeposition towards its adhesion strength. The optical images in Table 2 illustrate the thin Cu films generated on etched and unetched FTO glass following the tape-test procedure shown.

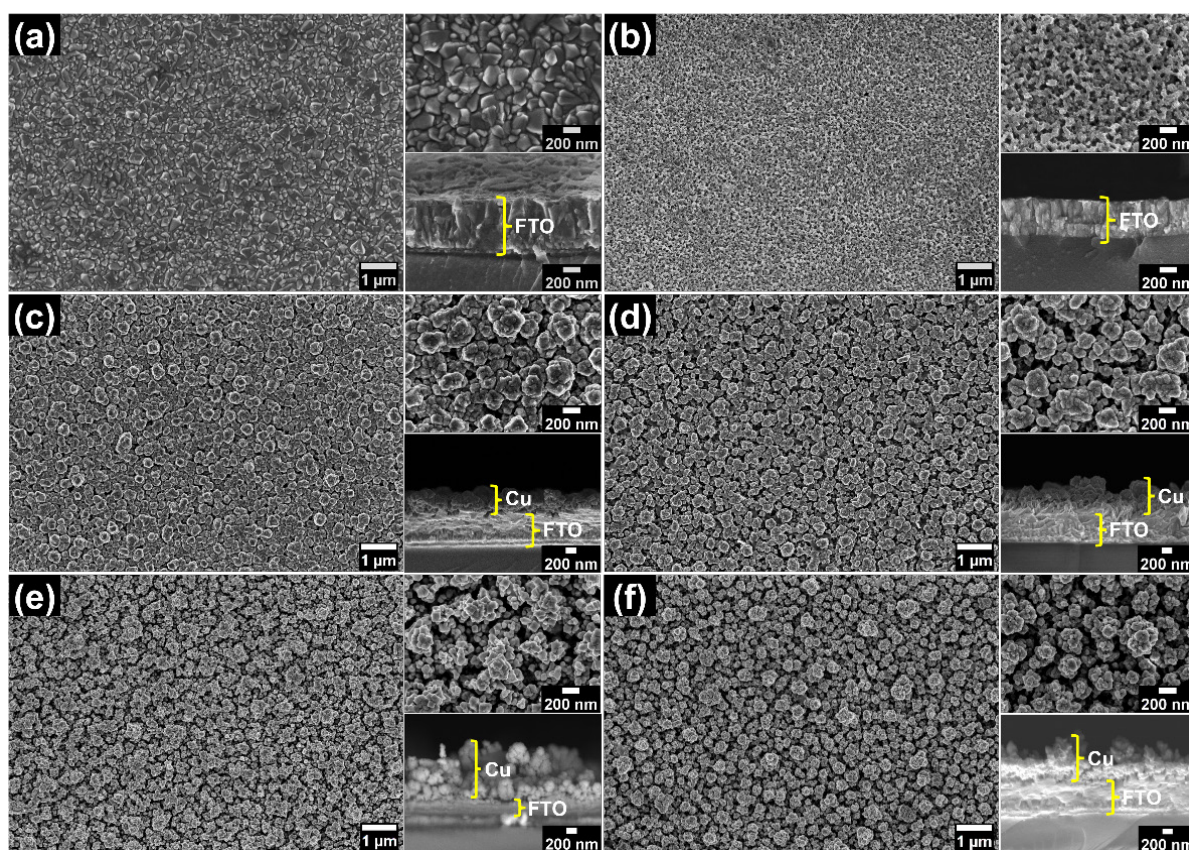


FIGURE 6. FESEM images of (a) blank FTO substrate, (b) etched FTO substrate, FTO/Cu electrodeposited at -0.4 V for (c) DD-600s-E, (d) PD-200cyc-E, and at -0.8 V for (e) DD-600s-E, and (f) PD-200cyc-E (main image is at 10k magnification, the inset shows the enlargement of the main image, and the cross section both at 50k magnification)

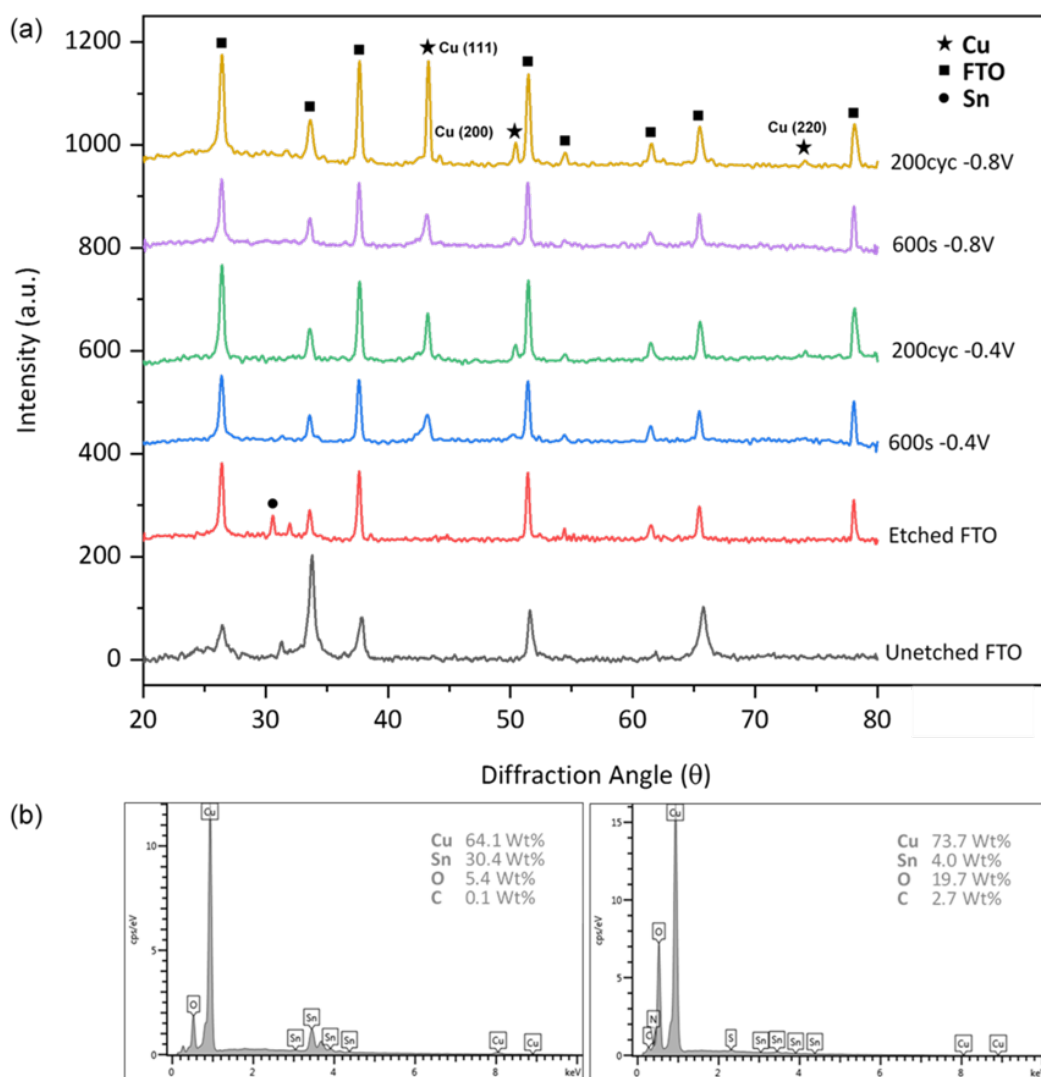


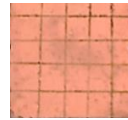
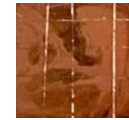
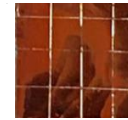
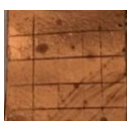
FIGURE 7. (a) XRD Spectra of the FTO-Cu prepared via DD and PD on etched FTO substrate, and EDX spectrum of (b) FTO/Cu DD-E at -0.4 V (left) and at -0.8 V (right) (*FTO/Cu PD-E has similar EDX pattern)

The Cu deposited on unetched FTO glass exhibits a high propensity for detachment from the FTO glass surface. This detachment can occur either partially, resulting in partial deposition on the tape, when a voltage of -0.8V is applied, or completely, leading to full deposition on the tape, when a voltage of -0.4V is applied. Regarding the electrochemical deposition of Cu on the etched FTO glass at a voltage of -0.4V, it was observed that the Cu layer exhibited strong adhesion to the FTO glass substrate. Consequently, the application of the adhesive tape did not cause any discernible modifications to the Cu layer. Nevertheless, the application of a voltage of -0.8V for the deposition of Cu onto etched FTO glass

resulted in the subsequent peeling of the Cu layer during the tape test. This peeling phenomenon can be attributed to the formation of a powdery Cu layer on the FTO glass surface during the electrodeposition process at -0.8V.

In contrast to etched FTO, unetched FTO glass exhibits diminished adhesion strength between a thin copper layer and the FTO glass. During the process of electrolysis reduction of FTO glass, it has been observed that the SnO_2 layers experience discoloration and dissolution in the presence of an acidic solution. These changes have a significant impact on the enhancement of adhesion strength, as reported by Laverty, Feng and Maguire (1997) and Liu et al. (1994). According to a

TABLE 2. Tape-test of adhesion strength between FTO glass and thin Cu film

		Deposition voltage (-0.4V)				Deposition voltage (-0.8V)			
		DD 600s	DD 600s-E	PD 200cyc	P 200cyc-E	DD 600s	DD 600s-E	PD 200cyc	PD 200cyc-E
After tape test	Before tape test								
	FTO Substrate								
	Peeled Tape								

study conducted by More and Bhargava (2017), the use of etched FTO enables the deposition of copper within the porous structure of FTO. Hence, the integration of an electrolysis reduction process as an etching treatment can result in enhanced adhesion between a thin Cu film and FTO glass.

Based on previous studies on the electrodeposition of copper onto unetched FTO substrates, it is anticipated that the predominant binding mechanism between copper and FTO is physical adsorption (Khelladi et al. 2009). This mechanism is thought to be accountable for the observed low strength of adhesion between the two materials. On the other hand, the increase in adhesion strength between Cu and etched FTO observed during the tape test can be ascribed to the interlocking mechanism, which is facilitated by the uneven surface topography and higher pore density of FTO. The results mentioned above align with previous studies that have shown the influence of surface roughness on both mechanical interlocking and adhesion strength (Lim, Lee & Chen 2017).

CONCLUSIONS

This study has demonstrated the formation of primarily spherical nanostructured Cu deposited onto FTO glass by direct voltage electrodeposition (DD) and pulsed voltage electrodeposition (PD) methods with the presence of inorganic additive Na_2SO_4 . Metallic thin Cu film was deposited at the voltage of -0.4V, meanwhile at the voltage of -0.8V, giving powdery thin Cu films. The

Cu grain size also increased when DD time increased from the 60s to 600s. The grain size also increased when the PD cycles were increased to 200 cycles from 50 cycles. PD is preferable in obtaining denser and more compact Cu structures than DD. The deposition of nanostructured Cu metal on FTO glass was confirmed by EDX and XRD spectrum. The etching of FTO glass before electrodeposition improved the adhesion strength between Cu deposited and the FTO glass substrate.

ACKNOWLEDGMENTS

The authors would like to thank the Ministry of Higher Education, Malaysia for the Fundamental Research Grant Scheme (FRGS-1-2020-STG04-UKM-02-5) and Universiti Kebangsaan Malaysia for providing the facilities and research grant (GUP-2022-078).

REFERENCES

- Adolf, J.D. 2008. *Function of Additives in Copper Electrodeposition for Semiconductor Devices Metallization*. Case Western Reserve University. Department of Chemical Engineering, Ed. Case Western Reserve University. <https://books.google.com.my/books?id=CqqzDAEACAAJ>
- Alfadhli, S., Darwish, A. A. A., Soliman, S., El-Zaidia, E. F. M., Yahia, I. S., Laariedh, F., Alatawi, A., Bahamran, A., Alatawi, N.M. & Hamdalla, T.A. 2023. Structural characterizations and photoelectric performance of non-crystalline boron subphthalocyanine chloride films/FTO for photodiode applications. *Journal of Non-Crystalline Solids* 601: 122044. doi:10.1016/j.jnoncrsol.2022.122044

- Alshehri, A.A. & Malik, M.A. 2020. Facile one-pot biogenic synthesis of Cu-Co-Ni trimetallic nanoparticles for enhanced photocatalytic dye degradation. *Catalysts* 10(10): 1138. doi:10.3390/catal10101138
- Aravinda, C.L., Mayanna, S.M. & Muralidharan, V.S. 2000. Electrochemical behaviour of alkaline copper complexes. *Journal of Chemical Sciences* 112(5): 543-550. doi:10.1007/BF02709287
- Babouri, L., Belmokre, K., Kabir, A., Abdelouas, A., Khettabi, R. & El Mendili, Y. 2019. Microstructure and crystallographic properties of Cu 77 Zn 21 alloy under the effect of heat treatment. *Materials at High Temperatures* 36(2): 165-172. doi:10.1080/09603409.2018.1499243
- Bae, J.W., Koo, B.R., An, H.R. & Ahn, H.J. 2015. Surface modification of fluorine-doped tin oxide films using electrochemical etching for dye-sensitized solar cells. *Ceramics International* 41(10): 14668-14673. doi:10.1016/j.ceramint.2015.07.189
- Bakthavatsalam, R., Ghosh, S., Biswas, R.K., Saxena, A., Raja, A., Thotiyl, M.O., Wadhai, S., Banpurkar, A.G. & Kundu, J. 2016. Solution chemistry-based nano-structuring of copper dendrites for efficient use in catalysis and superhydrophobic surfaces. *RSC Advances* 6: 8416-8430. doi:10.1039/C5RA22683J
- Böhme, A., Sterl, F., Kath, E., Ubl, M., Manninen, V. & Giessen, H. 2019. Electrochemistry on inverse copper nanoantennas: Active plasmonic devices with extraordinarily large resonance shift. *ACS Photonics* 6(8): 1863-1868. doi:10.1021/ACSPHOTONICS.9B00716
- Borkar, R., Dahake, R., Rayalu, S. & Bansiwala, A. 2018. Copper oxide nanograss for efficient and stable photoelectrochemical hydrogen production by water splitting. *Journal of Electronic Materials* 47(3): 1824-1831. doi:10.1007/s11664-017-5966-y
- Braesch, G., Oshchepkov, A.G., Bonnefont, A., Asonkeng, F., Maurer, T., Maranzana, G., Savinova, E.R. & Chatenet, M. 2020. Nickel 3D structures enhanced by electrodeposition of nickel nanoparticles as high performance anodes for direct borohydride fuel cells. *ChemElectroChem* 7(7): 1789-1799. doi:10.1002/celec.202000254
- Calcutt, V. 2001. August. *Copper Applications in Metallurgy of Copper & Copper Alloys*. Copper Development Association Inc.
- Chaitra, U., Muhammed Ali, A.V., Mahesha, M.G., Kompa, A., Kekuda, D. & Mohan Rao, K. 2021. Property evaluation of spin coated Al doped ZnO thin films and Au/AZO/FTO Schottky diodes. *Superlattices and Microstructures* 155: 106903. doi:10.1016/j.spmi.2021.106903
- Chang, T.W., Tseng, C.C., Chen, D.W., Wu, G., Yang, C.L. & Chen, L.C. 2021. Preparation and characterization of thin-film solar cells with Ag/C60/MAPbI3/CZTSe/Mo/FTO multilayered structures. *Molecules* 26(12): 3516. doi:10.3390/molecules26123516
- Chen, H., Yang, T., Liu, F. & Li, W. 2019. Electrodeposition of gold nanoparticles on Cu-based metal-organic framework for the electrochemical detection of nitrite. *Sensors and Actuators B: Chemical* 286: 401-407. doi:10.1016/j.snb.2018.10.036
- Danilovic, N., Subbaraman, R., Strmcnik, D., Chang, K.C., Paulikas, A.P., Stamenkovic, V.R. & Markovic, N.M. 2012. Enhancing the alkaline hydrogen evolution reaction activity through the bifunctionality of Ni(OH)₂/metal catalysts. *Angewandte Chemie* 124(50): 12663-12666. doi:10.1002/ange.201204842
- Das, M.K., Urumarudappa, S.K.J., Kamal, S., Widiadita, Y., Mahamud, A., Saito, T.I. & Bovornratanaraks, T. 2022. Effect of pulse electrodeposition parameters on the microstructure and mechanical properties of Ni-W/B nanocomposite coatings. *Nanomaterials* 12(11): 1871. doi:10.3390/nano12111871
- Dubale, A.A., Pan, C.J., Tamirat, A.G., Chen, H.M., Su, W.N., Chen, C.H., Rick, J., Ayele, D.W., Aragaw, B.A., Lee, J.F., Yang, Y.W. & Hwang, B.J. 2015. Heterostructured Cu₂O/CuO decorated with nickel as a highly efficient photocathode for photoelectrochemical water reduction. *Journal of Materials Chemistry A* 3(23): 12482-12499. doi:10.1039/C5TA01961C
- Esmaili, S., Bahrololoom, M.E. & Kavanagh, K.L. 2011. Electrodeposition, characterization and morphological investigations of NiFe/Cu multilayers prepared by pulsed galvanostatic, dual bath technique. *Materials Characterization* 62(2): 204-210. doi:10.1016/j.matchar.2010.11.017
- Grujicic, D. & Pesic, B. 2002. Electrodeposition of copper: The nucleation mechanisms. *Electrochimica Acta* 47(18): 2901-2912. doi:10.1016/S0013-4686(02)00161-5
- Gu, C.D., You, Y.H., Wang, X.L. & Tu, J.P. 2012. Electrodeposition, structural, and corrosion properties of Cu films from a stable deep eutectics system with additive of ethylene diamine. *Surface and Coatings Technology* 209: 117-123. doi:10.1016/j.surfcoat.2012.08.047
- Gyftou, P., Pavlatou, E.A. & Spyrellis, N. 2008. Effect of pulse electrodeposition parameters on the properties of Ni/nano-SiC composites. *Applied Surface Science* 254(18): 5910-5916. doi:10.1016/j.apsusc.2008.03.151
- Haba, T., Ikeda, K. & Uosaki, K. 2019. Electrochemical and *in situ* SERS study of the role of an inhibiting additive in selective electrodeposition of copper in sulfuric acid. *Electrochemistry Communications* 98: 19-22. doi:10.1016/J.ELECOM.2018.11.007
- Han, Y.J., Zhang, X. & Leach, G.W. 2014. Shape control of electrodeposited copper films and nanostructures through additive effects. *Langmuir* 30(12): 3589-3598. doi:10.1021/LA500001J
- He, J., Feng, H., Wang, T., Wang, T. & Zeng, H. 2018. Morphology-controlled electrodeposition of copper nanospheres onto FTO for enhanced photocatalytic hydrogen production. *Chinese Journal of Chemistry* 36(1): 31-36. doi:10.1002/cjoc.201700344
- Huang, L.J., Zhang, G.M., Zhang, Y., Li, B.J., Ren, N.F., Zhao, L. & Wang, Y.L. 2021. Preparation and photoelectric properties of patterned Ag nanoparticles on FTO/glass substrate by laser etching and driving layer strategy. *Acta Metallurgica Sinica (English Letters)* 34(7): 973-985. doi:10.1007/s40195-020-01169-y

- Jaikumar, A., Santhanam, K.S.V., Kandlikar, S.G., Raya, I.B. & Raghupathi, P. 2015. Electrochemical deposition of copper on graphene with high heat transfer coefficient. *ECS Transactions* 66(30): 55-64. doi:10.1149/06630.0055ecst
- Jeong, D., Jo, W., Jeong, J., Kim, T., Han, S., Son, M.K. & Jung, H. 2022. Characterization of Cu₂O/CuO heterostructure photocathode by tailoring CuO thickness for photoelectrochemical water splitting. *RSC Advances* 12(5): 2632-2640. doi:10.1039/D1RA08863G
- Jothi, L., Jaganathan, S.K. & Nageswaran, G. 2020. An electrodeposited Au nanoparticle/porous graphene nanoribbon composite for electrochemical detection of alpha-fetoprotein. *Materials Chemistry and Physics* 242: 122514. doi:10.1016/j.matchemphys.2019.122514
- Kaewvilai, A., Tanathakorn, R., Laobuthee, A., Rattanasakulthong, W. & Rodchanarowan, A. 2017. Electroless copper plating on nano-silver activated glass substrate: A single-step activation. *Surface and Coatings Technology* 319: 260-266. doi:10.1016/J.SURFCOAT.2017.04.018
- Kannimuthu, K., Sangeetha, K., Sam Sankar, S., Karmakar, A., Madhu, R. & Kundu, S. 2021. Investigation on nanostructured Cu-based electrocatalysts for improving water splitting: A review. *Inorganic Chemistry Frontiers* 8(1): 234-272. doi:10.1039/D0QI01060J
- Keshtmand, R., Zamani-Meymian, M.R., Mohamadkhani, F. & Taghavinia, N. 2021. Smoothing and coverage improvement of SnO₂ electron transporting layer by NH₄F treatment: Enhanced fill factor and efficiency of perovskite solar cells. *Solar Energy* 228: 253-262. doi:10.1016/j.solener.2021.09.068
- Khan, H., Yerramilli, A.S., D'Oliveira, A., Alford, T.L., Boffito, D.C. & Patience, G.S. 2020. Experimental methods in chemical engineering: X-ray diffraction spectroscopy - XRD. *The Canadian Journal of Chemical Engineering* 98(6): 1255-1266. doi:10.1002/cjce.23747
- Khaniche, B., Zouaoui, A. & Zegadi, A. 2020. Structural study and electrochemical deposition of a copper layer on n-Si. *Emerging Materials Research* 9(2): 1-6. doi:10.1680/jemmr.19.00051
- Khelladi, M.R., Mentar, L., Azizi, A., Sahari, A. & Kahoul, A. 2009. Electrochemical nucleation and growth of copper deposition onto FTO and n-Si(100) electrodes. *Materials Chemistry and Physics* 115(1): 385-390. doi:10.1016/j.matchemphys.2008.12.017
- Kim, E.K., Yoon, S.J., Bui, H.T., Patil, S.A., Bathula, C., Shrestha, N.K., Im, H. & Han, S.H. 2020. Epitaxial electrodeposition of single crystal MoTe₂ nanorods and Li⁺ storage feasibility. *Journal of Electroanalytical Chemistry* 878: 114672. doi:10.1016/j.jelechem.2020.114672
- Kim, G.H., Woo, H., Kim, S., An, T. & Lim, G. 2020. Highly-robust, solution-processed flexible transparent electrodes with a junction-free electrospun nanofiber network. *RSC Advances* 10(17): 9940-9948. doi:10.1039/C9RA10278G
- Kotok, V.A., Malyshev, V.V., Solovov, V.A. & Kovalenko, V.L. 2017. Soft electrochemical etching of FTO-coated glass for use in Ni(OH)₂-based electrochromic devices. *ECS Journal of Solid State Science and Technology* 6(12): P772-P777. doi:10.1149/2.0071712jss
- Laverty, S.J., Feng, H. & Maguire, P. 1997. Adhesion of copper electrodeposited to thin film tin oxide for electrodes in flat panel displays. *J. Electrochem. Soc.* 144(6): 2166-2170.
- Lee, K., Kim, A.Y., Park, J.H., Jung, H.G., Choi, W., Lee, H.Y. & Lee, J.K. 2014. Effect of micro-patterned fluorine-doped tin oxide films on electrochromic properties of Prussian blue films. *Applied Surface Science* 313: 864-869. doi:10.1016/j.apsusc.2014.06.092
- Li, B. & Zhang, W. 2020. Facile synthesis and electrochemical properties of a novel Ni-B/TiC composite coating via ultrasonic-assisted electrodeposition. *Ultrasonics Sonochemistry* 61: 104837. doi:10.1016/j.ultsonch.2019.104837
- Li, J., Zhou, Y.H., Zhong, D.Y., Li, X.F. & Zhang, J.H. 2019. Simultaneous enhancement of electrical performance and negative bias illumination stability for low-temperature solution-processed SnO₂ thin-film transistors by fluorine incorporation. *IEEE Transactions on Electron Devices* 66(10): 4205-4210. doi:10.1109/TED.2019.2936484
- Li, X., Natsuki, J. & Natsuki, T. 2021. "Sandwich" copper nanoparticle @ graphene oxide composites: High-Temperature stability and long-term stable conductivity. *Materials Characterization* 172: 110887. doi:10.1016/j.matchar.2021.110887
- Lim, J.D., Lee, P.M. & Chen, Z. 2017. Understanding the bonding mechanisms of directly sputtered copper thin film on an alumina substrate. *Thin Solid Films* 634: 6-14. doi:10.1016/j.tsf.2017.05.005
- Liu, J.S., Laverty, S.J., Maguire, P., McLaughlin, J. & Molloy, J. 1994. The role of an electrolysis reduction in copper-electroplating on transparent semiconductor tin oxide. *Journal of The Electrochemical Society* 141(4): L38-L40. doi:10.1149/1.2054872
- Luo, J., Steier, L., Son, M.K., Schreier, M., Mayer, M.T. & Grätzel, M. 2016. Cu₂O nanowire photocathodes for efficient and durable solar water splitting. *Nano Letters* 16(3): 1848-1857. doi:10.1021/ACS.NANOLETT.5B04929/SUPPL_FILE/NL5B04929_SI_001.PDF
- Maduraiveeran, G., Sasidharan, M. & Jin, W. 2019. Earth-abundant transition metal and metal oxide nanomaterials: Synthesis and electrochemical applications. *Progress in Materials Science* 106: 100574. doi:10.1016/j.pmatsci.2019.100574
- Mandke, M.V. & Pathan, H.M. 2012. Electrochemical growth of copper nanoparticles: Structural and optical properties. *Journal of Electroanalytical Chemistry* 686: 19-24. doi:10.1016/j.jelechem.2012.09.004
- Mathur, J. 2013. Effect of electrodeposition parameters on morphology of copper thin films. *IOSR Journal of Engineering* 3(8): 55-61. doi:10.9790/3021-03835561

- Mentar, L. 2011. Early stages of cobalt-copper alloys electrodeposition onto fluorine-doped tin oxide electrodes in sulfate solution. *Oriental Journal of Chemistry* 27(2): 477-483.
- Mladenović, I.O., Bošković, M.V., Vuksanović, M.M., Nikolić, N.D., Lamovec, J.S., Vasiljević-Radović, D.G. & Radojević, V.J. 2022. Structural, mechanical and electrical characteristics of copper coatings obtained by various electrodeposition processes. *Electronics* 11(3): 443. doi:10.3390/electronics11030443
- More, V. & Bhargava, P. 2017. Electrodeposited copper current collecting fingers for DSSCs. *Materials Science in Semiconductor Processing* 68: 178-185. doi:10.1016/j.mssp.2017.05.013
- Nasirpour, F., Alipour, K., Daneshvar, F. & Sanaeian, M.R. 2020. Electrodeposition of anticorrosion nanocoatings. In *Corrosion Protection at the Nanoscale*, edited by Rajendran, S., Nguyen, T.A., Kakooei, S., Yeganeh, M. & Li, Y. Elsevier. pp. 473-497. doi:10.1016/b978-0-12-819359-4.00024-6
- Nikolić, N.D. & Popov, K.I. 2010. Hydrogen co-deposition effects on the structure of electrodeposited copper. In *Electrodeposition. Modern Aspects of Electrochemistry*, edited by Djokic, S. New York: Springer. 48: 1-70. doi:10.1007/978-1-4419-5589-0_1
- Norzehana, N., Isa, C., Mohd, Y., Hafizuddin, M., Zaki, M., Aminah, S. & Mohamad, S. 2017. Electrodeposition and characterization of copper coating on stainless steel substrate from alkaline copper solution containing ethylenediaminetetraacetate (EDTA). *Journal of Mechanical Engineering* 2(1): 127-138.
- Odetola, P., Popoola, P., Popoola, O. & Delpont, D. 2016. Parametric variables in electro-deposition of composite coatings. *Electrodeposition of Composite Materials*. InTech. doi:10.5772/62010
- Olson, T.S., Atanassov, P. & Brevnov, D.A. 2005. Electrodeposition of gold particles on aluminum substrates containing copper. *The Journal of Physical Chemistry B* 109(3): 1243-1250. doi:10.1021/jp045670w
- Oo, T.Z., Devi Chandra, R., Yantara, N., Prabhakar, R.R., Wong, L.H., Mathews, N. & Mhaisalkar, S.G. 2012. Zinc Tin Oxide (ZTO) electron transporting buffer layer in inverted organic solar cell. *Organic Electronics* 13(5): 870-874. doi:10.1016/j.orgel.2012.01.011
- Pan, J., Zhang, Z., Zhan, Z., Xiong, Y., Wang, Y., Cao, K. & Chen, Y. 2020. *In situ* generation of silver nanoparticles and nanocomposite films based on electrodeposition of carboxylated chitosan. *Carbohydrate Polymers* 242: 116391. doi:10.1016/j.carbpol.2020.116391
- Pavlović, M.G., Pavlović, L.J., Maksimović, V.M., Nikolić, N.D. & Popov, K.I. 2010. Characterization and morphology of copper powder particles as a function of different electrolytic regimes. *Int. J. Electrochem. Sci.* 5: 1862-1878. www.electrochemsci.org.
- Qing, Y., Hu, C., Yang, C., An, K., Tang, F., Tan, J. & Liu, C. 2017. Rough structure of electrodeposition as a template for an ultrarobust self-cleaning surface. *ACS Applied Materials & Interfaces* 9(19): 16571-16580. doi:10.1021/acsmi.6b15745
- Qiu, R., Cha, H.G., Noh, H.B., Shim, Y.B., Zhang, X.L., Qiao, R., Zhang, D., Kim, Y.I., Pal, U. & Kang, Y.S. 2009. Preparation of dendritic copper nanostructures and their characterization for electroreduction. *The Journal of Physical Chemistry C* 113(36): 15891-15896. doi:10.1021/jp904222b
- Rajput, A., Kundu, A. & Chakraborty, B. 2021. Recent progress on copper-based electrode materials for overall water-splitting. *ChemElectroChem* 8(10): 1698-1722. doi:10.1002/celec.202100307
- Rana, M.S., Rahman, M.A. & Alam, A.M.S. 2014. A CV study of copper complexation with guanine using glassy carbon electrode in aqueous medium. *ISRN Electrochemistry* 2014: 1-7. doi:10.1155/2014/308382
- Rashidi, A.M. & Amadeh, A. 2008. The effect of current density on the grain size of electrodeposited nanocrystalline nickel coatings. *Surface and Coatings Technology* 202(16): 3772-3776. doi:10.1016/j.surfcoat.2008.01.018
- Rasouli, F., Rouhollahi, A. & Ghahramanifard, F. 2019. Gradient doping of copper in ZnO nanorod photoanode by electrodeposition for enhanced charge separation in photoelectrochemical water splitting. *Superlattices and Microstructures* 125: 177-189. doi:10.1016/j.spmi.2018.08.026
- Ren, N., Wang, W., Li, B., Huang, L. & Zhang, Y. 2021. Preparation and property optimization of silver-embedded FTO transparent conductive thin films by laser etching and coating AZO layer. *Journal of Materials Science: Materials in Electronics* 32(8): 10644-10661. doi:10.1007/s10854-021-05720-0
- Riveros, G., León, M., Ramírez, D., Hernández, L., Martín, F., Romero, R. & Dalchiale, E.A. 2020. Study of the nucleation and growth mechanisms of copper electrodeposition on bare and nitrogen-doped reduced graphene oxide modified SnO₂/F/glass substrates. *Journal of The Electrochemical Society* 167(12): 122508. doi:10.1149/1945-7111/abb281
- Sadana, Y.N., Deshpande, A.K. & Gedye, R.N. 1982. Electrodeposition of alloys XIII: Electrodeposition of Cu-Ni alloys from solutions containing L-asparagine. *Surface Technology* 17(2): 111-123. doi:10.1016/0376-4583(82)90013-9
- Schiavi, P.G., Farina, L., Zanoni, R., Altimari, P., Cojocariu, I., Rubino, A., Navarra, M.A., Panero, S. & Pagnanelli, F. 2019. Electrochemical synthesis of nanowire anodes from spent lithium ion batteries. *Electrochimica Acta* 319: 481-489. doi:10.1016/j.electacta.2019.07.024
- Schnebele, E., Jaiswal, K., Luco, N. & Nassar, N.T. 2019. Natural hazards and mineral commodity supply: Quantifying risk of earthquake disruption to South American copper supply. *Resources Policy* 63: 101430. doi:10.1016/j.resourpol.2019.101430

- Sekar, R. 2017. Synergistic effect of additives on electrodeposition of copper from cyanide-free electrolytes and its structural and morphological characteristics. *Transactions of Nonferrous Metals Society of China* 27(7): 1665-1676. doi:10.1016/S1003-6326(17)60189-4
- Shivakumara, S., Manohar, U., Arthoba Naik, Y. & Venkatesha, T.V. 2007. Influence of additives on electrodeposition of bright Zn-Ni alloy on mild steel from acid sulphate bath. *Bulletin of Materials Science* 30(5): 455-462. doi:10.1007/s12034-007-0072-z
- Smith, J.R., Campbell, S.A. & Walsh, F.C. 1995. Cyclic voltammetry at metal electrodes. *Transactions of the IMF* 73(2): 72-78. doi:10.1080/00202967.1995.11871062
- Taheraslani, M. & Gardeniers, H. 2019. High-resolution SEM and EDX characterization of deposits formed by CH₄+Ar DBD plasma processing in a packed bed reactor. *Nanomaterials* 9(4): 589. doi:10.3390/nano9040589
- Tang, M.H., Chakthranont, P. & Jaramillo, T.F. 2017. Top-down fabrication of fluorine-doped tin oxide nanopillar substrates for solar water splitting. *RSC Advances* 7(45): 28350-28357. doi:10.1039/C7RA02937C
- Tao, P., Chen, Y., Cai, W. & Meng, Z. 2021. Effect of copper sulfate and sulfuric acid on blind hole filling of hdi circuit boards by electroplating. *Materials* 14(1): 1-11. doi:10.3390/MA14010085
- Tarditi, A.M., Bosko, M.L. & Cornaglia, L.M. 2017. 3.1 Electroless plating of Pd binary and ternary alloys and surface characteristics for application in hydrogen separation. *Comprehensive Materials Finishing* 3-3: 1-24. doi:10.1016/B978-0-12-803581-8.09166-9
- Toupin, J., Strub, H., Kressmann, S., Boudot, M., Artero, V. & Laberty-Robert, C. 2017. Engineering n-p junction for photo-electrochemical hydrogen production. *Physical Chemistry Chemical Physics* 19(45): 30675-30682. doi:10.1039/c7cp05122k
- Tran, D.T.T., Nguyen, D.Q., Pham, C.H., Tran, L.D. & Nguyen, D.T. 2020. Facile synthesis of CuO/ITO film via the chronoamperometric electrodeposition for nonenzymatic glucose sensing. *Communications in Physics* 3(2): 161. doi:10.15625/0868-3166/30/2/14801
- Veerakumar, P., Sangili, A., Manavalan, S., Thanasekaran, P. & Lin, K.C. 2020. Research progress on porous carbon supported metal/metal oxide nanomaterials for supercapacitor electrode applications. *Industrial & Engineering Chemistry Research* 59(14): 6347-6374. doi:10.1021/acs.iecr.9b06010
- Vuong, D.T., Hoang, H.M., Tran, N.H. & Kim, H.C. 2020. Pulsed electrodeposition for copper nanowires. *Crystals* 10(3): 218. doi:10.3390/cryst10030218
- Wahyudi, S., Soepriyanto, S., Mubarak, M.Z. & Sutarno. 2019. Effect of pulse parameters on the particle size of copper powder electrodeposition. *IOP Conference Series: Materials Science and Engineering* 547(1): 012020. doi:10.1088/1757-899X/547/1/012020
- Wang, K., Ke, X., Wang, W., Tu, C., Luo, D. & Zhang, M. 2020. The impacts of fluorine-doped tin oxide photonic crystals on a cadmium sulfide-based photoelectrode for improved solar energy conversion under lower incidence. *Catalysts* 10(11): 1252. doi:10.3390/catal10111252
- Xu, Y., Zhu, J., Feng, J., Wang, Y., Wu, X., Ma, P., Zhang, X., Wang, G. & Yan, X. 2021. A rechargeable aqueous zinc/sodium manganese oxides battery with robust performance enabled by Na₂SO₄ electrolyte additive. *Energy Storage Materials* 38: 299-308. doi:10.1016/j.ensm.2021.03.019
- Yun, Y., Dong, Z., Shanov, V. N., Doepke, A., Heineman, W. R., Halsall, H. B., Bhattacharya, A., Wong, D.K.Y. & Schluz, M.J. 2008. Fabrication and characterization of carbon nanotube array electrodes with gold nanoparticle tips. *Sensors and Actuators B: Chemical* 133(1): 208-212. doi:10.1016/j.snb.2008.02.019
- Zhang, J., Han, J., Shi, Z., Ju, Y., Zhang, Z. & Gu, M. 2019. Fabrication and enhanced H₂O₂-sensing properties of the uniform porous FTO glasses with tunable pore sizes and densities. *Applied Surface Science* 465: 357-361. doi:10.1016/j.apsusc.2018.09.191
- Zhang, Z., Jiang, C., Cai, F., Fu, P., Ma, N. & Ji, V. 2015. Two stages for the evolution of crystallite size and texture of electrodeposited Ni-ZrC composite coating. *Surface and Coatings Technology* 261: 122-129. doi:10.1016/j.surfcoat.2014.11.048
- Zhao, G., Xuan, J., Liu, X., Jia, F., Sun, Y., Sun, M., Yin, G. & Liu, B. 2019. Low-cost and high-performance ZnO nanoclusters gas sensor based on new-type FTO electrode for the low-concentration H₂S gas detection. *Nanomaterials* 9(3): 435. doi:10.3390/nano9030435
- Zhao, J., Sun, L., Canepa, S., Sun, H., Yesibolati, M.N., Sherburne, M., Xu, R., Sritharan, T., Loo, J.S.C., Ager III, J.W., Barber, J., Mølhave, K. & Xu, Z.J. 2017. Phosphate tuned copper electrodeposition and promoted formic acid selectivity for carbon dioxide reduction. *Journal of Materials Chemistry A* 5(23): 11905-11916. doi:10.1039/C7TA01871A

*Corresponding author; email: lorna_jm@ukm.edu.my